UCRL-17126

University of California

Ernest O. Lawrence Radiation Laboratory

STRUCTURE ANALYSIS OF LOW ENERGY ELECTRON DIFFRACTION PATTERNS USING AN OPTICAL ANALOG

TWO-WEEK LOAN COPY

This is a Library Circulating Copy which may be borrowed for two weeks. For a personal retention copy, call Tech. Info. Division, Ext. 5545

DISCLAIMER

This document was prepared as an account of work sponsored by the United States Government. While this document is believed to contain correct information, neither the United States Government nor any agency thereof, nor the Regents of the University of California, nor any of their employees, makes any warranty, express or implied, or assumes any legal responsibility for the accuracy, completeness, or usefulness of any information, apparatus, product, or process disclosed, or represents that its use would not infringe privately owned rights. Reference herein to any specific commercial product, process, or service by its trade name, trademark, manufacturer, or otherwise, does not necessarily constitute or imply its endorsement, recommendation, or favoring by the United States Government or any agency thereof, or the Regents of the University of California. The views and opinions of authors expressed herein do not necessarily state or reflect those of the United States Government or any agency thereof or the Regents of the University of California.

TECHNICAL INFORMATION DIVISION

Radiation Laboratory

Berkeley

Assigned to INFORMATION DIVISION

Route to	Noted
B.V. Pyle	JUN 26 1967

Please return this document to the Information Division. Do not send it to the next person on the list.

Please do not remove this page.

RL-254-1

To be submitted to Acta Crystallographica

UCRL-17126
Preprint

UNIVERSITY OF CALIFORNIA

Lawrence Radiation Laboratory
Berkeley, California

AEC Contract W-7405-eng-48

STRUCTURE ANALYSIS OF LOW ENERGY ELECTRON DIFFRACTION PATTERNS USING AN OPTICAL ANALOG

A. Chutjian and G. A. Somorjai

January 1967

Structure Analysis of Low Energy Electron Diffraction Patterns Using an Optical Analog

A. Chutjian and G. A. Somorjai

Department of Chemistry of the
University of California and the
Inorganic Materials Research Division
of the Lawrence Radiation Laboratory,
Berkeley, California 94720

Abstract

Use is made of the principles of Fraunhofer diffraction to simulate low energy electron diffraction (LEED) pattern intensities from the (100) crystal face of platinum for the purposes of surface structure analysis. The model considers diffraction by ten atomic planes having 50 atoms in each (100) plane. The effects of different atomic scattering factors, attenuation of the electron beam between planes, and expansion and contraction of the topmost surface plane with respect to underlying atomic planes have been considered. The intensities of fractional order

diffraction spots which are due to ordered arrays of a) surface atoms, or b) surface vacancies have been calculated. A computer program for the intensity analysis is developed using ten planes of an f.c.c. lattice and a surface plane of atoms or vacancies. Instrumental and surface effects which could influence the coherence length of the scattered electron beam have also been discussed.

Although the position and width of the diffraction spots can be explained by our treatment, the intensities of the fractional order diffraction spots due to the Pt(100)-(5x1) surface structure is higher than predicted by this simple model.

Contents

Abstract iii

1. Introduction 1

2. Experimental Method 2

3. Some Simple Fourier Transforms 3

4. Analogy Between LEED and Optical Diffraction 5

   A. Diffraction Coordinates 6

   B. Coherency 10

5. Computation of the Scattered Intensity by Bulk & Surface Layers 14

   A. Surface Structures 16

6. The Atomic Scattering Factor 19

7. Correlation of Experimental and Theoretical Intensities . . . 20

   A. Intensity vs. Angle 20

   B. Intensity vs. Beam Voltage 24

8. Conclusions 25

Acknowledgements 26

Appendix 27

References 33

Figure Captions 34

1. Introduction

Low energy electron diffraction has been eminently successful in recent years to probe the structure of solid surfaces. Electrons, due to their large scattering amplitude and low energy, back-reflect from the surface without penetrating more than a few atomic planes[1] below the surface plane. Thus, when diffracted, the resulting diffraction pattern is mainly characteristic of the arrangement of surface atoms.

Recent results indicate[2,3] that the properties of atoms at the surface are different from bulk properties. The surface may be considered as a separate phase in which atoms have different mean displacements (Debye-Waller factor) and there is a net contraction or expansion which gives rise to different lattice spacing. Due to these and other physical properties the surface atoms may undergo structural rearrangements (i.e. phase transformations) at temperatures where no such changes occur in the bulk. In addition, adsorbed gas atoms were also found to form a variety of surface structures as a function of coverage, crystal-face orientation and temperature.[1]

Low energy electron diffraction (LEED) is able to detect these structural changes at the surface. Thus, it plays the same role in understanding the properties of surfaces as x-ray diffraction for probing the structure of the bulk. A satisfactory physical model of the electron-surface interaction which can explain the intensities of the observed diffraction spots has not been developed as yet. Several attempts have been made recently, among which the theory of multiple scattering[4] is the most prominent.

The purpose of this paper is to develop a kinematic model using the optical analog which could be used to analyze LEED patterns. We shall show how the variation of the physical parameters which characterize our model (variation of lattice spacing, electron transmission coefficient) influence the calculated diffraction intensities. Two different models (atom and vacancy) have been used to simulate the intensities of the fractional order diffraction spots which are due to the experimentally observed Pt(100)-(5x1) surface structure. Changes in the diffracted beam intensities due to variation of the atomic scattering factor have also been computed.

Since we are primarily interested in comparing relative intensities of the calculated diffraction patterns which are functions only of the variables of our model, the effect of lattice vibrations (Debye-Waller factor) on the intensities has been neglected.

2. Experimental Method

The experimental procedures using the post-acceleration technique are described thoroughly elsewhere.[1,5] For our purposes, the important points are the following: a beam of electrons having a variable energy of 5 to 500 eV strikes one face of a single crystal. The experiment is carried out in ultrahigh vacuum as to avoid contamination of the surface due to gas adsorption.* The back-diffracted electrons are screened to

---

* A crystal surface will adsorb a monolayer of foreign gas at 10^{-6} torr in one second (assuming a sticking coefficient of unity) so that typical operating pressures in the diffraction chamber are 10^{-10} torr to allow reasonable observation times.

eliminate the inelastically-scattered fraction, and accelerated towards a hemispherical fluorescent screen which detects and displays the diffraction pattern. The crystal can be rotated so that the specularly reflected fraction of electrons (I_{oo}) which would otherwise be directed back into the electron gun, can also be displayed on the screen. All observations are made through a 6" port in the forward direction.

3. Some Simple Fourier Transforms

In order to visualize the symmetry of the LEED patterns it is useful to consider the Fourier transforms of some discrete objects from real to reciprocal space. Buerger[6] has calculated transforms of a lattice row, lattice plane and three dimensional lattice, and his treatment can be summarized as follows. If the points along a lattice row in one dimension are spaced $\vec{a}$ apart, than all points in the row are given by $\vec{T}(1) = m\vec{a}$ where m is an integer. The Fourier transform of $\vec{T}(1)$ is $R(1) = \sum_{m=-\infty}^{\infty} e^{2\pi i\, m\vec{a}\cdot\vec{t}^*} = \sin \pi(2m+1)\vec{a}\cdot\vec{t}^*/\sin \pi\, \vec{a}\cdot\vec{t}^*$, where t^* is the reciprocal lattice vector. This function has maxima where $\vec{a}\cdot\vec{t}^*$ has integral values, and defines a set of planes in reciprocal space of spacing $t^* = 0, (1/a), 2(1/a), \ldots$ etc, normal to the lattice row. Where $\vec{T}$ is 2-dimensional; i.e., $\vec{T}(2) = m\vec{a} + n\vec{b}$, the reciprocal $R(2) = R(1)\cdot \sin \pi(2n+1)\vec{b}\cdot\vec{t}^*/\sin \pi\vec{b}\cdot\vec{t}^*$. The two factors have maxima where independently $\vec{a}\cdot\vec{t}^*$, $\vec{b}\cdot\vec{t}^* = 0, 1, 2, \ldots$. The locus of the intersection of the two mutually perpendicular planes is a set of parallel lines or rods which are normal to the crystal (ab) plane, and which intersect

the crystal at points of the reciprocal lattice. In 3-dimensions, $\vec{T}(3) = m\vec{a} + n\vec{b} + p\vec{c}$, and $\vec{R}(3) = R(1)\cdot R(2)\cdot \sin \pi(2p+1)\vec{c}\cdot\vec{t}^*/\sin \pi\vec{c}\cdot\vec{t}^*$. The third dimension has added another set of planes again mutually perpendicular to the first two, and the maxima in $\vec{R}(3)$ are now at the points of intersections of the parallelapipeds spaced 1/a, 1/b, 1/c, which comprise the reciprocal lattice.

The low energy electron diffraction pattern appears when the electrons which are elastically back-reflected from the crystal surface intercept the spherical fluorescent screen at a distance (~7 cm) much greater than the electron wavelength ($0.5 - 5\times10^{-8}$ cm). Diffraction by a single row of atoms produces lines on the screen which are the intersections of the diffraction planes, normal to the row, and the screen. Diffraction by a single atomic plane gives rise to spots at the intersection of the reciprocal lattice rods with the screen. (One characteristic of this two dimensional diffraction is that changing the wavelength of the impinging electron beam at constant electron density does not effect the intensity of the diffraction spots, although their position is altered.) Diffraction by a three dimensional lattice gives rise to the diffraction spots which appear, however, only at well-defined wavelengths at which all three Laue conditions of diffraction are met.

The case encountered in LEED is in most cases intermediate to the 2- and 3-dimensional examples. Whereas in x-ray diffraction the photon "feels" all three dimensions of the crystal, and the intensity maxima are given by $\vec{R}(3)$, the low-energy electrons "see" primarily the 2-dimensional surface and at most a depth of 10-15 planes. Therefore

the two dimensional diffraction features which are given by $\vec{R}(2)$ are strongly developed, and the LEED patterns are formed by the intersection of the reciprocal rods with the fluorescent screen. At low electron energies (~5-150 eV) the third Laue condition, being only weakly developed, causes fluctuations of the intensity of the diffraction spots as a function of electron wavelength. As the electron beam penetrates deeper into the crystal at higher beam voltages, the three dimensional character of low energy electron diffraction becomes more pronounced.

4. Analogy Between LEED and Optical Diffraction

The reciprocals $\vec{R}$ of the discrete points and plane of points are similar to the functions which govern the intensity distribution in the Fraunhofer plane by diffraction from periodic obstacles.

Following the treatment of Born and Wolf[7] and Stone,[8] the amplitude distribution in the Fraunhofer plane can be expressed as the product of the scattering by a single obstacle, and the coherent superposition of scattered waves from each obstacle. In the X-ray and LEED terminology the effect due to the interaction of a single atom with the impinging wave is described by the atomic scattering factor while the superposition of scattered waves from each atom is the symmetry factor. The product of the two is the structure factor.

4A. Diffraction Coordinates

The scattering geometry is shown in Figure 1. The Fraunhofer plane is defined by the origin O and the $\xi\eta$ axes, while x_1y_1 and x_2y_2 define the first two planes of atoms with origins O_1 and O_2, respectively. $Q_1(x_1,y_1)$ and $Q_2(x_2,y_2)$ are obstacles in O_1 and O_2, while $S(\xi',\eta')$ and $P(\xi,\eta)$ are the source and diffraction points in the Fraunhofer plane.

The distance L is 7 cm, $z \sim 2$Å, $\lambda \sim 1.5$Å and $d \sim 3$Å, are typical conditions encountered in LEED experiments. The size r of the screen pattern in terms of the interatomic spacing d and the electron wavelength λ is $r \sim (\lambda/d)\ L \sim (1.5/3)\ 7 = 3.5$ cm. The total area of the crystal surface irradiated by the electron beam is $\sim 1\ mm^2$.

In order to show that we are in the Fraunhofer, rather than Fresnel diffraction limit, we write the distances R_1, R_2, R_{1o} and R_{2o} as

$$R_1^2 = (\xi' - x_1)^2 + (\eta' - y_1)^2 + L^2$$

$$R_2^2 = (\xi - x_1)^2 + (\eta - y_1)^2 + L^2$$

$$R_{1o}^2 = \xi'^2 + \eta'^2 + L^2$$

$$R_{2o}^2 = \xi^2 + \eta^2 + L^2$$

or that

$$R_1^2 = R_{1o}^2 - 2(\xi' x_1 + \eta' y_1) + x_1^2 + y_1^2$$

$$R_2^2 = R_{2o}^2 - 2(\xi x_1 + \eta y_1) + x_1^2 + y_1^2 \quad .$$

Since the irradiated dimensions of the crystal are small compared to R_{10} and R_{20}, we can expand R_1 and R_2 as

$$R_1 \sim R_{10} - \frac{\xi' x_1 + \eta' y_1}{R_{10}} + \frac{x_1^2 + y_1^2}{2R_{10}} - \frac{(\xi' x_1 + \eta' y_1)^2}{2R_{10}^3} + \ldots$$

and a similar expression can be obtained for R_2.

The evaluation of the Kirchoff integral over the area of the diffracting obstacle will be easier when the terms quadratic in x_1 and y_1 can be neglected. This case constitutes the Fraunhofer limit. According to Born and Wolf the quadratic terms may be dropped if the subsequent change in the phase angle $k(R_1+R_2)$ is much smaller than 2π; i.e., if $k(x_1^2 + y_1^2)/2R_{10} \ll 2\pi$. Typical dimensions are $x_1 = y_1 \sim 200$Å (see section on coherency), $R_{10} \sim 7$ cm, and $k = 2\pi/\lambda \sim 2\pi/1.5$Å, so that $k(x_1^2 + y_1^2)/2R_{10} = (2\pi/1.5)(8/14)\ 10^{-4} = 2.4 \times 10^{-4} \ll 2\pi$.

In order to calculate the geometric difference in path in terms of the coordinates of Figure 1, we express the square of the length L-z in terms of the lengths R'_{10} and R'_{20} between S and O_2, and P and O_2, respectively,

$$(L-z)^2 = R_{10}'^2 - \xi'^2 - \eta'^2 = R_1'^2 - (\xi' - x_2)^2 - (\eta' - y_2)^2 \qquad (1)$$

And for the diffracted beam

$$(L-z)^2 = R_{20}'^2 - \xi^2 - \eta^2 = R_2'^2 - (\xi - x_2)^2 - (\eta - y_2)^2 \qquad (2)$$

The path difference Δ_1 for the source beam is $\Delta_1 = R_1' - R_{10}$, where $R_{10}^2 = L^2 + \xi'^2 + \eta'^2$. Using R_1^2 from Eq. (1), we get

$$R_1'^2 - R_{10}^2 = (R_1' + R_{10})(R_1' - R_{10}) = \Delta_1(R_1' + R_{10})$$

so that

$$\Delta_1 = \frac{x_2^2 + y_2^2 + z^2}{R_1' + R_{10}} - \frac{2}{R_1' + R_{10}} (x_2\xi' + y_2\eta' + Lz)$$

Letting $R_1' + R_{10} \sim 2R_{10}$ and neglecting $x_2^2/2R_{10}$, we get

$$\Delta_1 = -\frac{1}{R_{10}} (x_2\xi' + y_2\eta' + Lz).$$

But $\xi'/R_{10} = \sin\theta_1$, $\eta'/R_{10} = \sin\phi_1$, and $L/R_{10} = \cos\zeta$ where $\cos\zeta = \cos\theta_1 \cos\phi_1$, so we get the final symmetric form

$$\Delta_1 = -(x_2 \sin\theta_1 + y_2 \sin\phi_1 + z \cos\zeta).$$

Similarly, we define the path difference Δ_2 for the diffracted beam as

$$\Delta_2 = R_2' - R_{10}$$

$$= -\frac{1}{R_{20}} (x_2\xi + y_2\eta + Lz)$$

and we define the analogous angles $\xi/R_{20} = \sin\theta_2$, $\eta/R_{20} = \sin\phi_2$, and $L/R_{20} = \cos\theta$ where $\cos\theta = \cos\theta_2 \cos\phi_2$. We then have

$$\Delta_2 = -(x_2 \sin\theta_2 + y_2 \sin\phi_2 + z \cos\theta).$$

If we adopt the notation that $\Delta_1{}^{\ell jp}$ and $\Delta_2{}^{\ell jp}$ are the phases of the $\ell j^{\underline{th}}$ atom in the $p^{\underline{th}}$ plane, then the coherent superposition of the phases $k\Delta_1{}^{\ell jp}$ and $k\Delta_2{}^{\ell jp}$ can be expressed as

$$A = \sum_{p=1}^{P} \sum_{j=1}^{N} \sum_{\ell=1}^{M} e^{-ki(\Delta_1{}^{\ell jp} + \Delta_2{}^{\ell jp})} \tag{3}$$

where the values of M, N, and P are as yet unspecified.

If we allow for the case in which the phases Δ_1 and Δ_2 are complex; i.e., when there is an attenuation of the incident and exiting electron beams as they pass through each plane, then the total phase is $k(\Delta_1{}^{\ell jp} + \Delta_2{}^{\ell jp}) - 2i(p-1)\epsilon$ where ϵ is an absorption coefficient per plane. If we let $\alpha = e^{-\epsilon}$, Eq. (3) can be written as

$$A = \sum_{p=1}^{P} \sum_{j=1}^{N} \sum_{\ell=1}^{M} \alpha^{2(p-1)} e^{-ik(\Delta_1{}^{\ell jp} + \Delta_2{}^{\ell jp})} \tag{4}$$

We can rewrite Eq. (4) in a more useful form[8] since x_j^ℓ and y_j^ℓ are periodic with spacings D_x and D_y, respectively, so that $x_j^\ell = (\ell-1)D_x$ and $y_j^\ell = (j-1)D_y$. Now let us define the phases δ_x and δ_y such that $\delta_x = \frac{kD_x}{2\Pi}(\sin\theta_1 + \sin\theta_2)$ and $\delta_y = (kDy/2\Pi)(\sin\phi_1 + \sin\phi_2)$, where $k = 2\Pi/\lambda$. Then, the corresponding sums in Eq. (4) become

$$A = \sum_{p=1}^{P} \sum_{j=1}^{N} \sum_{\ell=1}^{M} \alpha^{2(p-1)} e^{-2\Pi i(\ell-1)\delta_x} e^{-2\Pi i(j-1)\delta_y} e^{-ikz_p(\cos\zeta + \cos\theta)} \tag{5}$$

The sums over the atoms in the x-y plane can be expressed in a closed form[8] as

$$\sum_{j=1}^{N} \sum_{\ell=1}^{M} e^{-2\pi i(\ell-1)\delta_x} e^{-2\pi i(j-1)\delta_y} = e^{-\pi i(M-1)\delta_x} e^{-\pi i(N-1)\delta_y} \cdot$$

$$\times \frac{\sin M\pi\delta_x}{\sin \pi\delta_x} \cdot \frac{\sin N\pi\delta_y}{\sin \pi\delta_y} \tag{5a}$$

The scattering efficiency of the $\ell jp^{\underline{th}}$ atom into the angle θ is given by the atomic scattering factor $f_{\ell jp}(\lambda,\theta)$, and the structure factor becomes $F = f_{\ell jp}(\lambda,\theta)\cdot A$. Since in our case, for monatomic solids all atoms are identical, the subscripts on $f_{\ell jp}(\lambda,\theta)$ can be dropped and F can be written as

$$F = f(\lambda,\theta) e^{-i\pi[(M-1)\delta_x+(N-1)\delta_y]} \left\{ \frac{\sin M\pi\delta_x}{\sin \pi\delta_x} \cdot \frac{\sin N\pi\delta_y}{\sin \pi\delta_y} \right\}$$

$$\times \sum_{p=1}^{P} \alpha^{2(p-1)} e^{-ikz_p(\cos\zeta + \cos\theta)} \tag{6}$$

4B. <u>Coherency</u>

Up to this point nothing has been said about the limits N, M and P in the summation of Eq. (4). These limits will determine, respectively, the number of atoms in the surface plane (x,y) and the number of atomic planes (z) below the surface plane which have to be considered in

calculating the structure factor. We will show that a) the number of atoms in the x-y plane which diffract coherently can be estimated from the angular width of the diffraction spots and b) that the number of atomic planes in the z-direction which contribute to the scattering of electrons is a function of the attenuation factor, α.

a) Using the arguments of Born and Wolf,[7] let P_1 and P_2 be two points on the face of the crystal, and let the crystal be many wavelengths from the source. If P_1 and P_2 are closer than one wavelength, then the amplitude and phase of the electrons arriving at P_1 and P_2 will effectively be the same. Some correlation will exist even for greater separation of P_1 and P_2 until the distance Δl between them approaches the coherence length $v\Delta t \sim v/\Delta\nu$ of the electron beam, where $\Delta\nu$ is the spectral width of the beam, v the electron velocity and Δt the coherence time. The corresponding degree of coherence, or the visibility of the fringes from P_1 and P_2 will vary from unity (perfect correlation) to zero (no correlation).

Several estimates of the length Δl can be obtained from experimental data. At 150 eV, the wavelength of the electron is 1Å. If the spectral width is governed solely by the Maxwellian spread in energies of the electrons boiling off the cathode,[9] than at a filament temperature $T = 800°K$ electrons will be moving toward and away from the crystal with an average energy of $3/2\ kT$, and a total spread $\Delta(eV) = 3kT = 0.21$ eV, or $\Delta\lambda = 7 \times 10^{-4}$ Å. This may be a lower limit to the spread since we have neglected field distortions at the electron lenses, and space charge effects near the cathode. The corresponding upper limit to the coherence length on the crystal surface is then $v/\Delta\nu = \lambda^2/\Delta\lambda \sim 1400$ Å.

A criterion for the lateral coherence length follows from the Van Cittert-Zernicke Theorem[7] which states in part that the visibility of fringes from P_1 and P_2 will be 0.88 if the distance Δl between them is

$$\Delta l = 0.16 \frac{\lambda}{\alpha} \tag{7}$$

where α is the angular radius of the source at the crystal. For a filament-to-crystal distance of 20 cm, and a filament height of ~ 5 mm, $2\alpha = .5/20$, and $\Delta l \sim 13$ Å. Coherence length of the same magnitude can be calculated from the effect of the electron beam diameter (1 mm^2) on the width of the diffraction peaks.[10]

The angular width of the observed diffraction peaks also provide an estimate of the number of scattering centers which diffract coherently. The essential quantity from Eq. (6) which determines the height and width of the diffraction maxima is $F \sim \sin N\pi\delta/\sin \pi\delta$. If we move by a small amount δ' away from the $m^{\underline{th}}$ order, then $\delta = \delta' + m$, and $F = \sin N\pi\delta'/\sin \pi\delta' \sim \sin N\pi\delta'/\pi\delta'$. The point at which F^2 which is proportional to the intensity, I, is one-half its peak height of N^2 is then[8]

$$0.5 = \left(\frac{\sin N\pi\delta'}{N\pi\delta'}\right)^2$$

or $N\pi\delta' = 1.5$. Since $\delta' = (D/\lambda)\sin \Delta\theta_2 \sim (D/\lambda)\Delta\theta_2$, $\Delta\theta_2$, the half-width at half maximum, is given by

$$\Delta\theta_2 = \frac{1.5}{\pi N} \cdot \frac{\lambda}{D}$$

The normalized quantity $N \cdot \frac{D}{\lambda}$ is plotted against $\Delta\theta_2$ in Figure 2. In order to obtain N from experimental half-widths it is necessary to multiply the value from the graph by the ratio of the lattice spacing and wavelength. This value of N is again only a lower limit to the size of the diffracting units, and is accurate only for vanishing instrumental width. In the present study, the narrowest widths (half-width at half-maxima) of the diffraction spots of platinum surfaces that were observed were 0.3° at 100 eV, corresponding to ~ 40 scattering centers or ~ 120Å. Estimates by Khan, Hobson, and Armstrong[11] of the uncertainty in the x-y momentum of their electrons at 1 eV give $N > 20$, or $\Delta l > 60$ Å. An additional estimate by Park[10] from beam widths gives $\Delta l \sim 10^2$ Å.

Since one can observe the change (decrease) in the size of the diffraction spots upon annealing after ion-bombardment for example, the widths of the diffraction spots do not seem to be limited by the instrument. Thus, the variation of the spot size may conveniently be used to investigate the rate of ordering or disordering of surface atoms.

b) The limit, P, on the summation over atomic planes in the z-direction depends on the attenuation of the electron beam per plane. Gafner[12] used the attenuation coefficient in the form $\alpha = e^{-0.125z}$, and for z = 2.3 Å, $\alpha = 0.75$. For $\alpha = 0.6$ the contribution of the sixth atomic plane to the total scattered amplitude is $\leq 0.5\%$. For $\alpha = 0.8$, twelve planes should be taken into account before the contribution of the deepest plane drops to the same small value. We have varied α in the range $0.6 < \alpha < 0.8$ in our calculations of the diffraction intensities. The variation of α in this range has only a very small effect on the intensities of the diffraction peaks.

5. Computation of the Scattered Intensity by Bulk and Surface Layers

In the present treatment we have assumed a coherence length of 140 Å which gives a fringe visibility of 12% at $\lambda = 2$Å [using Eq. (7)]. These values were estimated from the diffraction patterns obtained from platinum surfaces.[2] Therefore in our computation the limits N and M were chosen to be N = 50 and M = 50, or a surface plane of 50 x 50 atoms. We sum over 10 atomic planes in the z-direction (P = 10) in order to take into account the scattering due to the bulk atoms.[1]

For the (100) and (110) faces of an FCC lattice the 2nd, 4th, 6th, ... planes are displaced by $\frac{1}{2}(D_x, D_y)$ relative to the 1st, 3rd, 5th, ... planes; i.e., alternate planes are staggered. The atomic positions in the even planes will now be $x_{\ell j} = [(\ell-1)D_x + \frac{1}{2} D_x]$ and $y_{\ell j} = [(j-1)D_y + \frac{1}{2} D_y]$.

Performing the sums in Eq. (5a) for atoms in the even planes we have, letting $S\theta = (\sin\theta_1 + \sin\theta_2)$, $S\phi = (\sin\phi_1 + \sin\phi_2)$, $S_x = \frac{1}{2} D_x$, $S_y = \frac{1}{2} D_y$,

$$\sum_{j=1}^{N'} \sum_{\ell=1}^{M'} e^{-2\pi i(\ell-1)\delta_x} e^{-2\pi i(j-1)\delta_y} e^{-kS_x S\theta} e^{-kS_y S\phi}$$

$$= e^{-\pi i[(M'-1)\delta_x + (N'-1)\delta_y]} e^{-ik[S_x S\theta + S_y S\phi]} \frac{\sin M'\pi\delta_x}{\sin \pi\delta_x} \frac{\sin N'\pi\delta_y}{\sin \pi\delta_y} \tag{8}$$

Whereas the x and y directions on the (100) face are equivalent, the pattern given by Eq. (8) would not show the inversion symmetry of a (100) face since the second factor is present only for the even layers. The problem was therefore "symmetrized" by reducing the size of the even planes by one row and column of atoms. By letting M' = M-1 and N' = N-1 in Eq. (8), we get for the phase factor of the right hand side of Eq. (8)

$$e^{-\pi i[(M-1)\delta_x + (N-1)\delta_y]} \; e^{-ik[(\frac{D_y}{2} - S_y)\, S\phi + (\frac{D_x}{2} - S_x)\, S\theta]} .$$

But since $\frac{D_y}{2} = S_y$, $\frac{D_x}{2} = S_x$, we obtain for the phase and amplitude of Eq. (8)

$$e^{-\pi i[(M-1)\delta_x + (N-1)\delta_y]} \; \frac{\sin(M-1)\pi\delta_x}{\sin \pi\delta_x} \; \frac{\sin(N-1)\pi\delta_y}{\sin \pi\delta_y} ,$$

the same result as obtained for odd planes. Finally, the sum over even and odd planes separately in Eq. (6) gives for the structure factor

$$F_{bulk} = f(\lambda,\theta)\; e^{-\pi i[(M-1)\delta_x + (N-1)\delta_y]} \left\{ \frac{\sin M\pi\delta_x}{\sin \pi\delta_x} \cdot \frac{\sin N\pi\delta_y}{\sin \pi\delta_y} \times \right.$$

$$\sum_{p=1(odd)}^{9} \alpha^{2(p-1)} \cdot e^{-ikz_p(\cos\zeta + \cos\theta)} + \frac{\sin(M-1)\pi\delta_x}{\sin \pi\delta_x} \cdot \frac{\sin(N-1)\pi\delta_y}{\sin \pi\delta_y} \times$$

$$\left. \sum_{p=2(even)}^{10} \alpha^{2(p-1)} \; e^{-ikz_p(\cos\zeta + \cos\theta)} \right\} \qquad (9)$$

From Eq. (9) we see that F_{bulk} has maxima of magnitude MN ~ (M-1)(N-1) when δ_x, δ_y = 0, ±1, ±2, ... independently; the corresponding diffraction peak is labeled by the value (δ_x, δ_y). Also, the rotation $\delta_x \rightarrow \delta_y$, $\delta_y \rightarrow -\delta_x$; and the inversion $\delta_x \rightarrow -\delta_x$, $\delta_y \rightarrow -\delta_y$ leave F_{bulk} invariant for both even and odd planes, so that the scattering amplitude now has the same symmetry as the (100) face. The phase factor preceding the quantity in braces is common to all planes - bulk and surface - and becomes unity when we later calculate the intensity.

5A. Surface Structures

In addition to the diffraction spots due to the (100) face and underlying atomic planes given by the maxima in Eq. (9), diffraction spots which reflect greater periodicity at the surface are observed in many LEED patterns.[1] These spots are due to larger lattice spacings. For example, $D'_x = 5D_x$, $D'_y = D_y$ (5x1 structure); $D'_x = 5D_x$, $D'_y = 5D_y$ (5x5 structure), etc. Although the following treatment could be used to analyze all n x m patterns for n, m =1, ... 5, the analysis of only the (5x1) pattern which occurs on the (100) face of FCC platinum will be discussed in detail.

The new periodicities will be viewed in two ways. If we let P_x and P_y be the periodicities in the x and y directions respectively, then a (P_x x P_y) pattern may be due to the presence of an atom at every ℓP_x, mP_y position, where ℓ = 1, 2, ... M/P_x, m = 1, 2, ... N/P_y; or to the removal of an atom (presence of a vacancy) at that position.

If we choose $P_x = 5$, $P_y = 1$, $M = N = 52$ (this value of M allows us to place all (P_x x P_y) structures symmetrically on the surface) then $M - 1 = N - 1 = 51$ and the top layer will be symmetric if we place atoms in the 1st, 6th, 11th .... 51st positions in the x-direction, and in every position in the y-direction, so that

$$A_{atoms} = \sum_{\ell=1}^{11} e^{-ik(\ell-1)5\delta_x} \sum_{j=1}^{51} e^{-ki(j-1)\delta_y} e^{-kiS_x S\theta} e^{-kiS_y S\phi}$$

$$= \frac{\sin 55\pi\delta_x}{\sin 5\pi\delta_x} \cdot \frac{\sin 51\pi\delta_y}{\sin \pi\delta_y} e^{-51\pi i(\delta_x + \delta_y)} \qquad (10)$$

The surface amplitude has maxima in the x-direction when $\delta_x = 0$, $\pm.2$, $\pm.4$, ...; and in the y-direction when $\delta_y = 0$, ± 1, ± 2, ..., giving the familiar "5x1" diffraction pattern.

The phase due to the spacing in the z-direction is $e^{-ikz_T(\cos\zeta + \cos\theta)}$ from Eq. (8), where z_T is now the spacing between the surface layer and the first bulk layer.

The <u>second</u> case to be considered is one in which an atom is removed at every (ℓP_x, mP_y) position. From a full 51 x 51 (1x1 structure) surface array, atoms at every 1st, 6th, 11th .... 51st position in the x-direction are removed, with atoms in the y-direction remaining. For this 5 x 1 vacancy case the diffraction amplitude from the surface becomes

$$A_{vac} = e^{-51\pi i(\delta_x + \delta_y)} \; e^{-ik\, z_T\, (\cos\zeta + \cos\theta)} \left\{ \left(\frac{\sin 51\pi\delta_x}{\sin \pi\delta_x} - \frac{\sin 55\pi\delta_x}{\sin 5\pi\delta_x} \right) \frac{\sin 51\pi\delta_y}{\sin \pi\delta_y} \right\} \tag{11}$$

Combining Eqs. (11) and (9) and using a suitable attenuation, α_T, of the electron beam between the surface and bulk layers, the total amplitude of diffraction from ten (100) planes and a surface plane consisting of vacancies in a (5x1) array is

$$F_{tot}(\lambda, \zeta, \theta) = f(\lambda, \theta) \left[A_{vac} + \alpha_T^{\,2} A_{bulk} \right] \tag{12}$$

The value of α_T depends on the value of α and σ, the fraction of the (51 x 51) surface sites occupied. For $\sigma = 1$ (1 x 1 surface structure) $\alpha_T = \alpha$, and for $\sigma = 0$ (no surface plane) $\alpha_T = 1$. A linear variation of α_T with σ was assumed, so that $\alpha_T = \sigma(\alpha-1) + 1$. For the (5x1) layer of atoms case, $\sigma_A = (51 \times 11)/(51 \times 51) = 0.22$, and $\alpha_T = 0.94$ for $\alpha = 0.75$; while for the same vacancy structure $\sigma_y = (51 \times 40)/(51 \times 51) = 0.78$ (or $1 - \sigma_A$), and $\alpha_T = 0.80$.

6. The Atomic Scattering Factor

Three forms of the atomic scattering factor, $f(\lambda,\theta)$, were used in the calculations, and are shown in Figure 3.

The first, given by Curve A, was simply $f(\theta) = 1$; i.e., the atoms are assumed to be efficient scatterers in all directions.

The second form (Curve B) was calculated from the first order Bessel function and is given as $|f(\theta)|^2 = (2J_1(x)/x)^2$ where $x = (2\pi/\lambda) \cdot a \sin(\pi-\theta)$. The parameter a, which in optical diffraction is the radius of the circular diffracting apertures, was determined by the following argument. Experimentally, a minimum in the atomic scattering factor is observed as a dark ring on the LEED screen. For the Pt (100) face, this ring is seen at an angle $\pi-\theta = 32°$ and at 350 eV ($\lambda \doteq 0.75$Å). The function $(J_1(x)/x)$ has its first minimum at $x = 1.22\pi$, so that $a = (1.22\pi/2\pi) \times (0.75/\sin 32°) = 0.86$Å.

Finally, Curve C was derived from the approximate partial phases calculated by Lander and Morrison.[2] If the ℓth phase is denoted by η_ℓ, then

$$f(\theta) = \frac{1}{2ik} \sum_{\ell=0}^{\infty} (2\ell + 1)(e^{2i\eta_\ell} - 1)\, P_\ell(\cos\theta) \qquad (13)$$

where P_ℓ is the ℓth Legendre polynomial. The phases were calculated for $\ell = 0$ to 7 for tungsten ($z = 74$) at 60 eV using the Thomas-Fermi-Dirac (TFD) potential and a form of the WKB approximation. Since the TFD potential changes only slightly on going from $z = 74$ to $z = 79$ (Pt), we felt that the use of the phases calculated for tungsten would suffice

as an example. That the calculations are crude is shown by the minimum in Curve C at ~ 24° and 60 eV. This minimum is not seen experimentally at 60 eV.

7. Correlation of Experimental and Theoretical Intensities

A computer program was written (see the Appendix) to compute the sums in Eqs. (9), (10), and (11) which are used in Eq. (12). The program also computed $f(\theta)$ from Eq. (13) for each scattering angle, and at each wavelength. The final output was in the form of a Cal-Comp plot of intensity (the squared magnitude of Eq. (11)) vs. θ_2, or intensity (I_{oo}) vs. beam voltage.

7A. Intensity vs. Angle

Several experimental intensity measurements of the (5x1) structure were available from the work in this laboratory. These scans included both brightness spot meter readings and densitometric tracings from photographic negatives.

The fractional order diffraction spot (5x1) intensities were, in general, strongly dependent on the heating and ion-bombardment history of the sample. The common element in all of them, however, is that when the spots are fully developed the intensity of the fractional order spots are comparable to the bulk-spot intensities and the bulk to higher order spot intensity ratios are reproducible. These fractional order spots are present only over a range of low (5-130 eV) beam energies. The results of a typical experimental scan along the $(\bar{1}\bar{1})$ to $(0\bar{1})$ direction are shown in Figure 4.

The relative peak intensities (on an arbitrary scale) of several brightness spot meter scans along the $(\bar{1}\bar{1})$ to $(0\bar{1})$ direction on the screen are given in Table I for the (100) face of Pt. The angle of the (00) spot with respect to the surface normal was determined experimentally. The beam voltage was 58 eV (λ = 1.609Å).

Typical results of our computations are also shown in Table I. These were obtained after adjustment of the various parameters. The values of α and z_T were varied and the spot intensity ratios $(.\bar{8}0)/(\bar{1}0)$, $(.\bar{8}0)/(00)$, $(.\bar{8}\bar{1})/(\bar{1}\bar{1})$ and $(.\bar{8}\bar{1})/(0\bar{1})$ calculated. The intensity ratios varied of the order of 10% with changes in α and α_T in the range of $\alpha = 0.75 \pm .15$. The intensity ratios varied by nearly two orders of magnitude with variation of z_T from 1 to 3Å, but were never uniformly of the order of unity as observed experimentally. Two values of z_T of 1.940Å and 2.105Å close to the normal bulk spacing of 1.962Å were nevertheless chosen to illustrate the results. These values are by no means unique, and many other values of z_T near the bulk value would have sufficed equally to give the same results.

The remaining parameter -- the shape of the atomic scattering factor -- was used in the forms shown in Figure 3. Its effect, as seen from Eq. (11), is to modulate the intensities of the diffraction spots, just as the single slit pattern in an optical diffraction grating modulates the various orders.

The combination of parameters listed in Table I are as follows:

(1) top plane of vacancies

(2) top plane of atoms

(A) $f(\theta)$ shown in Fig. 3, Curve A

(B) $f(\theta)$ shown in Fig. 3, Curve B

(C) $f(\theta)$ shown in Fig. 3, Curve C

(a) $z_T = 1.962$

(b) $z_T = 2.105$

(c) $z_T = 1.940$

A typical computer scan along the $(\bar{1}\bar{1})$-$(0\bar{1})$ direction is shown in Figure 5. The results clearly show that the intensities of the fractional order spots are in general lower than observed experimentally. The higher intensities were observed only in cases where the partial wave scattering factor $f(\theta)$ was used. The $(\bar{1}\bar{1})$ and $(0\bar{1})$ peaks appeared at a scattering angle $\pi-\theta = 22.2°$ and $23.7°$, respectively, while the higher order spots were in an angular region of $19.2°$ to $15.8°$. The minimum in $f(\theta)$ at $\sim 24°$ attenuated the $(\bar{1}\bar{1})$ and $(0\bar{1})$ peaks by a factor of 4-6 more than the higher order spots. The effect would disappear, for example, if the (00) spot were rotated so that all the orders fell in the range $23° - 26°$ about the minimum. The effect of the Bessel function (Curve B) was to enhance only slightly the intensity of the fractional order spots at the smaller angle (2bA vs. 2bB). Neither lattice expansion nor contraction (2aA vs. 2bA, and 1aC vs. 1cC) sufficed to raise the intensities to the experimental values.

Table I.

EXPERIMENTAL AND CALCULATED INTENSITIES OF THE (5x1) STRUCTURE

The notation for "Case" is explained in the test.

	Experimental					
	$(\bar{1}\bar{1})$	$(.\bar{8}\bar{1})$	$(.\bar{6}\bar{1})$	$(.\bar{4}\bar{1})$	$(.\bar{2}\bar{1})$	$(0\bar{1})$
	100	78	116	54	70	64
	100	52	68	30	46	58
	100	88	116	57	79	79
	100	71	84	55	59	118
	100	58	64	42	44	110
	Calculated					
Case						
1aA	100	2.9	2.6	2.6	2.8	101
1bA	100	6.6	6.0	5.3	5.3	257
1bB	100	7.7	7.4	6.5	5.9	243
1cC	100	17	26	23	11	44
1cA	100	2.7	2.8	2.3	2.5	110
2aA	100	6.9	6.7	6.6	7.0	107
2bA	100	8.9	9.7	11	12	198
2aC	100	41	68	61	28	47
2bB	100	10	12	14	14	187

7B. Intensity vs. Beam Voltage

Another possible correlation with experimental data exists with the scan of I_{oo} vs. beam voltage. The experimental results are shown in Figure 6 for a clean Pt (100) face after heating to 1140°. The (00) spot was 12° from the gun in this example. The corresponding computed maxima are shown by arrows in Figure 6. Their spacing is given by the relation

$$2\lambda = 2z \cos i \tag{13}$$

where z is the interplanar spacing and i the angle of incidence measured from the crystal normal. With z = 1.962Å and cos i = .995, λ_{max} = 3.88, 1.96, 1.30, .98, .78, .65, .56, ... Angstrom or 10, 39, 89, 158, 247, 355 and 483 eV, respectively, where no inner or contact potential correction has been applied. The experimental maxima occur at 55, 70, 89, 155, 240, 355 and 485 eV. In addition, there are many weak reflections at 115, 140, 182, 195, 270, and 500 eV, arising from diffractions within the crystal not predicted by Eq. (13). If multiples of 2z are used in Eq. (13), extra computed peaks do appear, but neither their intensity nor exact position correspond to the experimental results. McRae[4] has given a more detailed treatment of this aspect of LEED. He has calculated from Lax's[13] multiple scattering equations the effective field at the $i\mu^{th}$ atom, made up of the primary (plane wave) field and the field emitted by all of the atoms other than the given atom. The treatment predicts a resonance peak at low (~ 5 eV) energies, and both ordinary Bragg peaks, and secondary peaks of integral

or fractional order. These sécondary Bragg peaks appear to split into several components with rotation of the sample. The treatment in general emphasizes the importance of the scattered field from all the atoms due to the large atomic cross sections at low electron energies.

8. Conclusions

(1) Although the simple optical analogue to the LEED process predicts spot positions and variation of spot width with coherence area, it predicts fractional order intensities in the (5x1) structures that are a factor of 5-10 smaller than experimentally observed. The normalized intensities for both the surface atom and vacancy case gave only slightly different values.

(2) Both the form of the atomic scattering factor and variation of z, the lattice spacing normal to the surface plane, can affect strongly the calculated intensity ratios. Changes in the value of the attenuation factor, α, had only small influence ($\sim$ 10%) on the intensity ratios in the range $\alpha = 0.6 - 0.8$.

(3) The treatment predicts only the Bragg reflections in the I_{oo} vs. eV curve. A more detailed analysis involving higher order scattering, effects of inner potential corrections and the change in $f(\lambda, \theta)$ with beam voltage is necessary to obtain better agreement.

Acknowledgements

We are pleased to thank H. B. Lyon, Jr. for many suggestions and comments both on the experimental and theoretical aspects of this problem. One of us (A.C.) would also like to thank the Bell Telephone Laboratories, Murray Hill, New Jersey, for the generous use of their computer facilities for the latter part of this work.

This work was performed under the auspices of the United States Atomic Energy Commission.

Appendix

The following program was used to calculate the diffraction intensities, the atomic scattering factor by the partial wave method, and to plot the intensities vs. scattering angle on the Cal-Comp plotter at the Lawrence Radiation Laboratory. The program is written for the CDC 6600 Computer in Chippewa Fortran IV language. The running time on the CDC is approximately 20 sec.

The computed amplitude sums, as well as the atomic scattering factor, were checked at several angles by hand calculations. These hand calculations agreed with the computed results to within 10%.

Comment cards have been liberally used in the Fortran listing so that the operations of smaller sections of the various subprograms may be explained.

```
      PRØGRAM LEED(INPUT,ØUTPUT,TAPE98,TAPE99)
C
C  THIS PRØGRAM CØMPRISES TEN PLATINUM (100) PLANES, WITH A TØP PLANE
C  CØNSISTING ØF ATØMS ØR VACANCIES. ALL LATTICE DIMENSIØNS ARE ASSIGNED
C  THEIR X-RAY BULK VALUES, EXCEPT FØR THE Z-SPACING ØF THE SURFACE
C  PLANE WHICH IS LEFT VARIABLE.
C
      CØMMØN/DATZ/DX,DY,THETA1,PHI1,ALPHA,ALPHAT,Z(10),CØTHET,SCATT,
     *  CØZFT,THET,ZT1,ZT2,SIZE,PX,PY,ATMX1,ATMX2,ATMY1,ATMY2,HØLX1,
     * HØLX2,HØLY1,HØLY2
      CØMMØN/BLAT/WAVE
      DATA ZT1,ZT2/-2.105,0./
      DATA ALPHAT,ALPHA/0.94,0.75/
      DATA DX,DY,WAVE,THETA1,PHI1/2.775,2.775,1.609,-9.0,-9.2/
      DATA SIZE,PX,PY/52.,5.,1./
      DATA ATMX1,ATMX2,ATMY1,ATMY2,HØLX1,HØLX2,HØLY1,HØLY2/51.,0.,
     *  51.,0.,55.,0.,51.,0./
      DATA (Z(I),I=1,10)/0.,1.962,3.924,5.887,7.849,9.811,11.773,
     *  13.735,15.698,17.66/
       PRINT 57,   DX,DY,WAVE,THETA1,PHI1,PX,PY,ALPHA,ALPHAT,ZT1,ZT2,
     * SIZE,Z,ATMX1,ATMX2,ATMY1,ATMY2,HØLX1,HØLX2,HØLY1,HØLY2
   57 FØRMAT(1H1,4H DX=F8.4,4H DY=F8.4,6H WAVE=F8.4,8H THETA1=F8.4,
     * 6H PHI1=F8.4,4H PX=F5.0,4H PY=F5.0,/7H ALPHA=F8.2,8H ALPHAT=F8.2,
     * 5H ZT1=F8.4,5H ZT2=F8.4,6H SIZE=F5.0,/3H Z=10F8.4,/7H ATMX1=F5.0,
     *  7H ATMX2=F5.0,7H ATMY1=F5.0,7H ATMY2=F5.0,7H HØLX1=F5.0,
     *  7H HØLX2=F5.0,7H HØLY1=F5.0,7H HØLY2=F5.0)
      DIMENSIØN X(451),EF(451)
      PRINT 4
    4  FØRMAT(1H0,8X,6HTHETA2,11X,5HSCATT,28X,9HINTENSITY//)
C
C  ZERØTH ØRDER SCAN IN THETA2 THRØUGH THE (00) SPØT
C
      K=451
      M=2
      WHY=-PHI1
      PRINT 15,WHY
   15 FØRMAT(1H0,8X,5HPHI2=F8.3)
      DØ 88 L=1,451
      X(L)=0.1*FLØAT(L-271)
      EF(L)=EFINT(X(L),WHY,WAVE,M)
      PRINT 67,X(L),SCATT,EF(L)
   67 FØRMAT(5X,F10.2,5X,F10.2,25X,1PE14.5)
   88 CØNTINUE
      CALL GRAPH(X,EF,K,M,18HSCAN FRØM 00 TØ 10,6HTHETA2,9HINTENSITY)
C
C  MINUS FIRST ØRDER SCAN IN THETA2 THRØUGH THE 0M1 SPØT.
C
      WHY=-ASIN(WAVE/DY+SIN(0.0174533*PHI1))*57.29578
      PRINT 15,WHY
      PRINT 4
      DØ 89 L=1,451
      X(L)=0.1*FLØAT(L-271)
      EF(L)=EFINT(X(L),WHY,WAVE,M)
      PRINT 67,X(L),SCATT,EF(L)
   89 CØNTINUE
      CALL GRAPH(X,EF,K,M,20HSCAN FRØM 0M1 TØ 1M1,6HTHETA2,9HINTENSITY)
      CALL CCFND
      STØP
      END
```

```
      FUNCTIØN FFINT(THETA2,PHI2,WAVE,M)
C
C  THIS PRØGRAM SUMS THE DIFFRACTIØN AMPLITUDES FRØM THE BULK AND
C  SURFACE ATØMS IN THE RLGIØN ØF CØHERENCE, MULTIPLIES THE RESULT BY
C  THE ATØMIC SCATTERING FACTØR, AND FINALLY CØMPUTES THE SQUARED
C  MAGNITUDE ØF THE RESULT TØ GIVE THE INTENSITY.
C
      CØMPLEX AMP,SUMØ,SUME,ATØMIC,FTØPS1
      CØMMØN/DATZ/DX,DY,THETA1,PHI1,ALPHA,ALPHAT,Z(10),CØTHET,SCATT,
     * CØZET,THET,ZT1,ZT2,SIZE,PX,PY,ATMX1,ATMX2,ATMY1,ATMY2,HØLX1,
     * HØLX2,HØLY1,HØLY2
      CØSCAT=CØS(0.0174533*(THETA2-THETA1))*CØS(0.0174533*(PHI2-PHI1))
      SCATT=ACØS(CØSCAT)*57.29578
      CØTHET=CØS(0.0174533*THETA2)*CØS(0.0174533*PHI2)
      CØZET=CØS(0.0174533*THETA1)*CØS(0.0174533*PHI1)
      DELTAX=(DX/WAVE)*(SIN(0.0174533*THETA1)+SIN(0.0174533*THETA2))*
     * 3.14159
      DELTAY=(DY/WAVE)*(SIN(0.0174533*PHI1)+SIN(0.0174533*PHI2))*3.14159
      DENØMX=SIN(DELTAX)
      DENØMY=SIN(DELTAY)
      SIZEM1=SIZE-1.
      SINSX=SIN(SIZE*DELTAX)
      SINSY=SIN(SIZE*DELTAY)
      SINSX1=SIN(SIZEM1*DELTAX)
      SINSY1=SIN(SIZEM1*DELTAY)
      IF(DENØMX) 1,2,1
    1 EFX=SINSX/DENØMX
      EFXEV=SINSX1/DENØMX
      GØ TØ 3
    2 EFX=SIZE
      EFXEV=SIZEM1
    3 IF(DENØMY) 4,5,4
    4 EFY=SINSY/DENØMY
      EFYEV=SINSY/DENØMY
      GØ TØ 6
    5 EFY=SIZE
      EFYEV=SIZEM1
    6 SUME=(0.,0.)
      SUMØ=(0.,0.)
      DØ 33 K=1,10
      BETA=-(Z(K)/WAVE)*(CØTHET+CØZET)*6.28319
C
C  THE EVEN- AND ØDD-NUMBERED LAYERS HAVE THEIR ØWN PHASE DIFFERENCE.

      N=K.AND.1
      IF(N) 18,14,18
   14 SUME=SUME+CMPLX(CØS(BETA),SIN(BETA))*ALPHA**(2*(K-1))
      GØ TØ 33
   18 SUMØ=SUMØ+CMPLX(CØS(BETA),SIN(BETA))*ALPHA**(2*(K-1))
   33 CØNTINUE
      AMP=EFX*EFY*SUMØ+EFXEV*EFYEV*SUME
C
C  THE AMPLITUDE AND PHASE ØF THE SURFACE PLANE IS EVALUATED.
C
   17 BETAT1=-(ZT1/WAVE)*(CØTHET+CØZET)*6.28319
      SINPX=SIN(PX*DELTAX)
      SINPY=SIN(PY*DELTAY)
      IF(SINPX) 40,41,40
   40 VCNCX1=SIN(HØLX1*DELTAX)/SINPX
      GØ TØ 42
   41 VCNCX1=HØLX1/PX
   42 IF(SINPY) 43,44,43
```

```
43    VCNCY1=SIN(HØLY1*DELTAY)/SINPY
      GØ TØ 45
44    VCNCY1=HØLY1/PY
45    IF(DENØMX) 46,47,46
46    SURFX1=SIN(ATMX1*DELTAX)/DFNØMX
      GØ TØ 48
47    SURFX1=ATMX1
48    IF(DFNØMY) 49,50,49
49    SURFY1=SIN(ATMY1*DFLTAY)/DFNØMY
      GØ TØ 51
50    SURFY1=ATMY1
51    FTØPS1=VCNCX1*VCNCY1*CMPLX(CØS(BETAT1),SIN(BETAT1))
C
C     THE BULK AND SURFACE AMPLITUDES ARE ADDED, MULTIPLIED BY THE ATØMIC
C     SCATTERING FACTØR, AND THE RESULT SQUARED.
C
      AMP=FTØPS1+ALPHAT**2*AMP
      AMP=AMP*ATØMIC(SCATT,WAVE)
      EFINT=REAL(AMP)**2+AIMAG(AMP)**2
      RETURN
      END
```

```
      CØMPLEX FUNCTIØN ATØMIC(THETA,WAVE)
C
C  THE CØMPLEX ATØMIC SCATTERING FACTØR IS CØMPUTED BY THE METHØD ØF
C  PARTIAL WAVES.
C
       CØMPLEX TERM
      DIMENSIØN P(8),ETA(8)
      DATA (ETA(L),L=1,8)/13.7,11.18,8.04,5.47,2.83,1.07,.19,0./
C
C  THE SCATTERING ANGLE USED IN CALCULATING F(THETA) IS THE SUPPLEMENT
C  ØF THE ANGLE USED IN DEFINING THE LEED PATTERNS.
C
      SUPP=180.-THETA
      X=CØS(0.0174533*SUPP)
      P(1)=1.
      P(2)=X
      P(3)=1.5*X**2-0.5
      P(4)=2.5*X**3-1.5*X
      P(5)=(35.*X**4-30.*X**2+3.)/8.
      P(6)=(63.*X**5-70.*X**3+15.*X)/8.
      P(7)=(231.*X**6-315.*X**4+105.*X**2-5.)/16.
      P(8)=(1287.*X**7-2079.*X**5+945.*X**3-105.*X)/48.
      ATØMIC=(0.,0.)
      DØ 22 L=1,8
      TERM=WAVE*0.0795775*(0.,-1.)*CMPLX(CØS(2.*ETA(L))-1.,
     *    SIN(2.*ETA(L)))*(2.*FLØAT(L-1)+1.)*P(L)
      ATØMIC=ATØMIC+TERM
22    CØNTINUE
      RETURN
      END
```

```
      SUBRØUTINE GRAPH(X,Y,K,M,RG,RX,RY)
C
C  THIS SUBRØUTINE CALLS THE VARIØUS CAL-CØMP LIBRARY SUBRØUTINES WHICH
C  PLØT THE FINAL INTENSITIES AND ANGLES.
C
      CØMMØN/CCPØØL/XMIN,XMAX,YMIN,YMAX,CCXMIN,CCXMAX,CCYMIN,CCYMAX
      DIMENSIØN RØUND(4),X(1),Y(1),EF(1)
      DATA (RØUND(I),I=1,4)/1.,2.,2.5,5./
      DATA NRØUND,PART/4,12./
      CALL LINEUP(X,K,RØUND,NRØUND,PART,XMIN,XMAX)
      IF(M-1)  24,24,25
24    CALL LINEUP(Y,K,RØUND,NRØUND,PART,YMIN,YMAX)
      CALL CCGRID(1,IFIX(PART),6HNØLBLS,1,IFIX(PART))
      CALL CCLBL(IFIX(PART),IFIX(PART))
      CALL CCPLØT(X,Y,K,6HNØJØIN,1,1)
      CALL CCLTR(1140.,925.,0,1,5HJØB A)
       GØ TØ 26
25    CALL LINEUP(Y,K,RØUND,NRØUND,12.,YMIN,YMAX)
      CALL CCGRID(1,IFIX(PART),6HNØLBLS,1,12)
      CALL CCLBL(IFIX(PART),12)
      CALL CCPLØT(X,Y,K,4HJØIN,1,1)
      CALL CCLTR(1140.,950.,0,2,24HALPHA=0.75,LAMBDA=1.582A)
26    CALL CCLTR(1140.,975.,0,2,RG)
      CALL CCLTR(540.,5.,0,2,RX)
      CALL CCLTR(0.,560.,1,2,RY)
       CALL CCNEXT
      RETURN
      END
```

References

1. J. J. Lander, Progress in Solid State Chemistry, Ed. H. Reiss (Pergamon Press, New York, 1964).
2. H. B. Lyon, G. A. Somorjai, "Low Energy Electron Diffraction Study of the Clean (100), (111) and (110) Faces of Platinum," J. Chem. Phys. (to be published).
3. H. B. Lyon, G. A. Somorjai, J. Chem. Phys. 44, 3707 (1966).
4. E. G. Mc Rae, J. Chem. Phys. 45, 3258 (1966).
5. J. J. Lander, F. C. Unterwald, J. Morrison, Rev. Sci. Instr. 33, 782 (1962).
6. M. J. Buerger, Crystal Structure Analysis (John Wiley, New York, 1960), p. 417.
7. M. Born and E. Wolf, Principles of Optics (3rd Edition, Pergamon, New York, 1965), p. 400.
8. J. M. Stone, Radiation and Optics (McGraw-Hill, New York, 1963), Ch. 7.
9. R. D. Heidenreich, Fundamentals of Transmission Electron Microscopy (Interscience, New York, 1964), Ch. 10.
10. R. L. Park, J. Appl. Phys. 37, 295 (1966).
11. I. H. Khan, J. P. Hobson, R. A. Armstrong, Phys. Rev. 129, 1513 (1963).
12. G. Gafner, Surface Science 2, 534 (1964).
13. M. Lax, Phys. Rev. 85, 621 (1952).

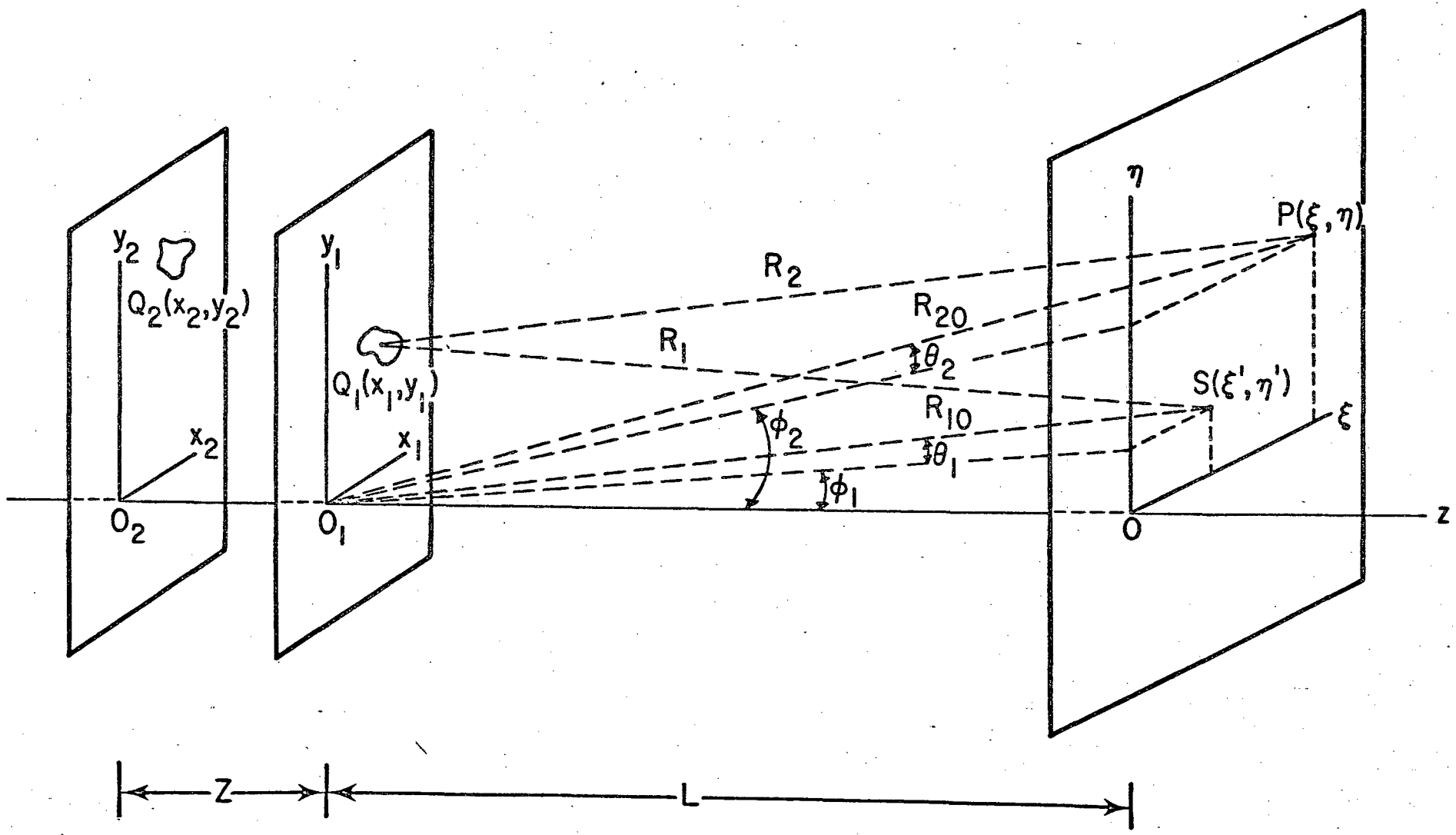

Figure 1. Geometry used in the derivation of Eq. (4). S is the electron gun source, P a point on the LEED screen, Q_1 and Q_2 two diffracting centers in planes O_1 and O_2, respectively.

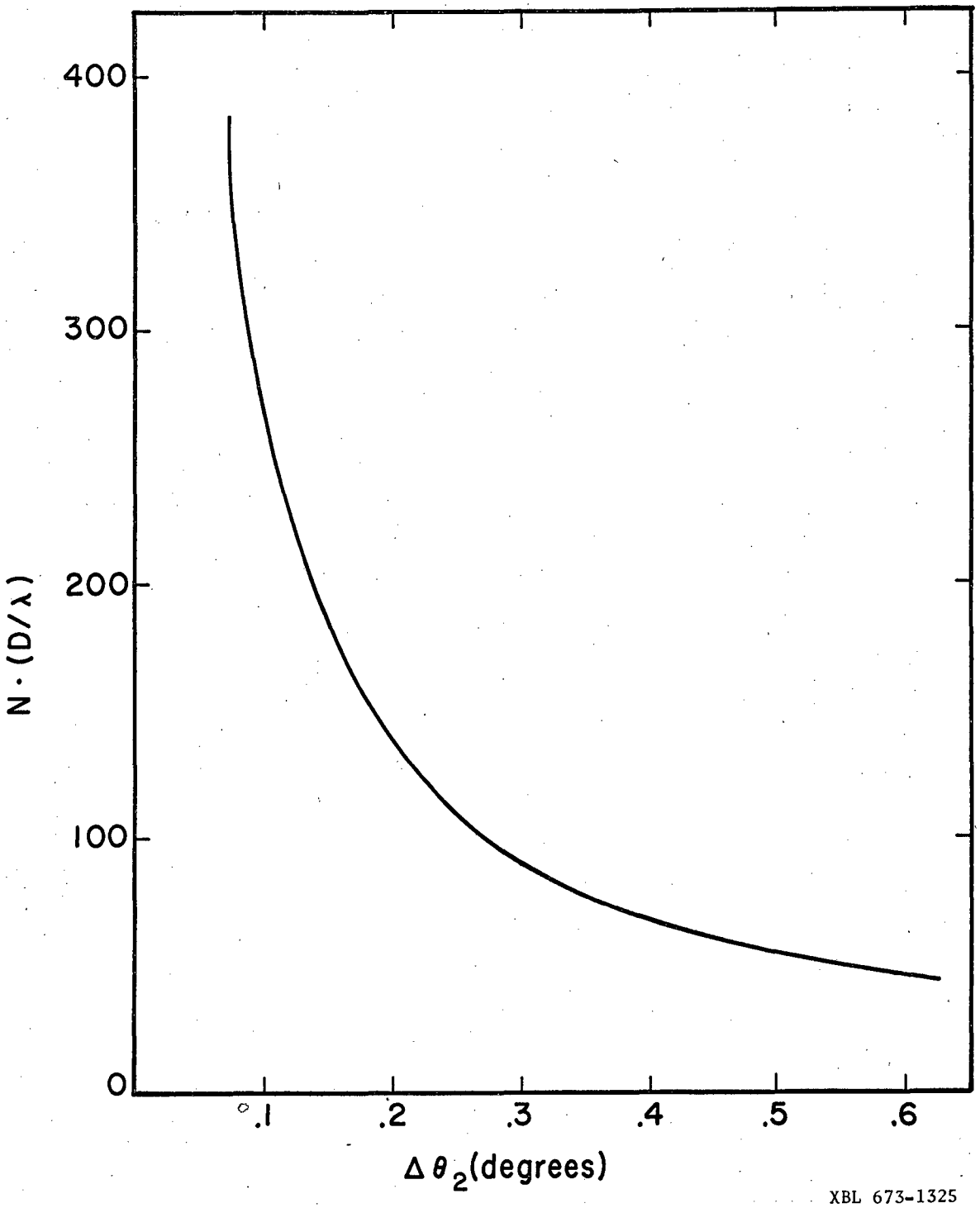

XBL 673-1325

Figure 2. Relationship between spot half-width at half-maximum $\Delta\theta_2$ and the number N of scattering centers. The value of N is normalized by the ratio of the x- or y-direction lattice spacing, D_1 and the wavelength λ.

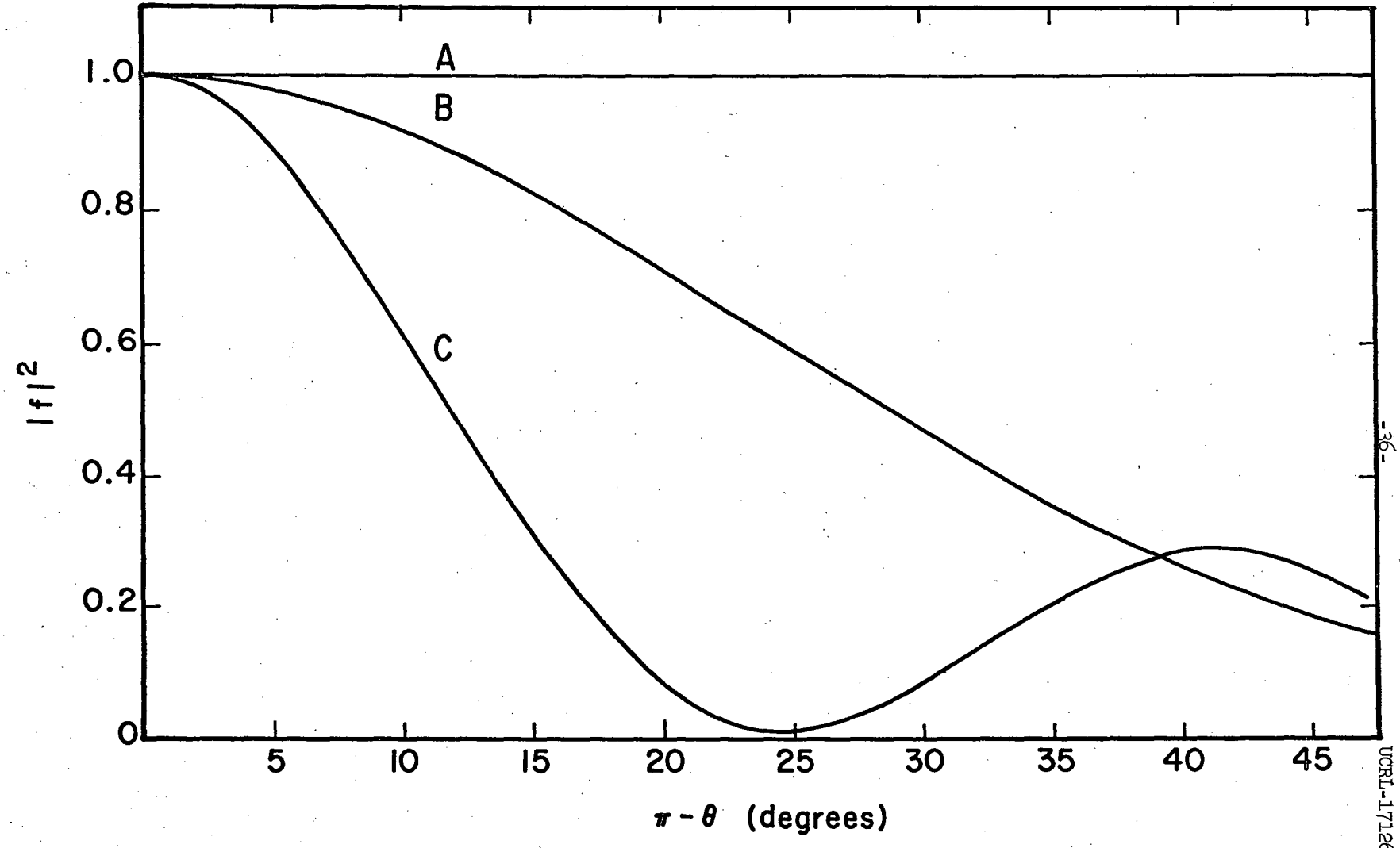

XBL 673-1323

Figure 3. Forms of the atomic scattering factor used. Curve A: $|f(\theta)|^2$ as unity. Curve B: $|f(\theta)|^2$ as $(J_1(x)/x)^2$. Curve C: $|f(\theta)|^2$ as the partial wave value.

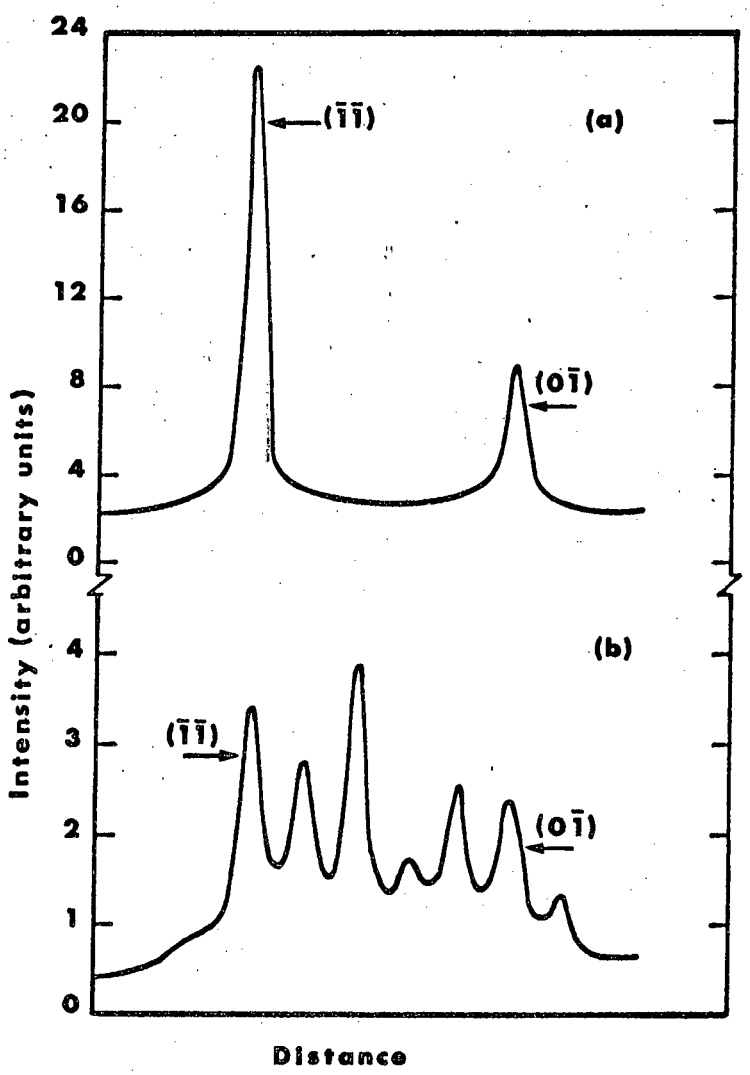

Figure 4. Experimental plot of intensity vs. distance (related to the angle θ_2) along the $(\bar{1}\bar{1})$-$(0\bar{1})$ direction in the (a) absence and in the (b) presence of the Pt(100)-(5x1) surface structure.

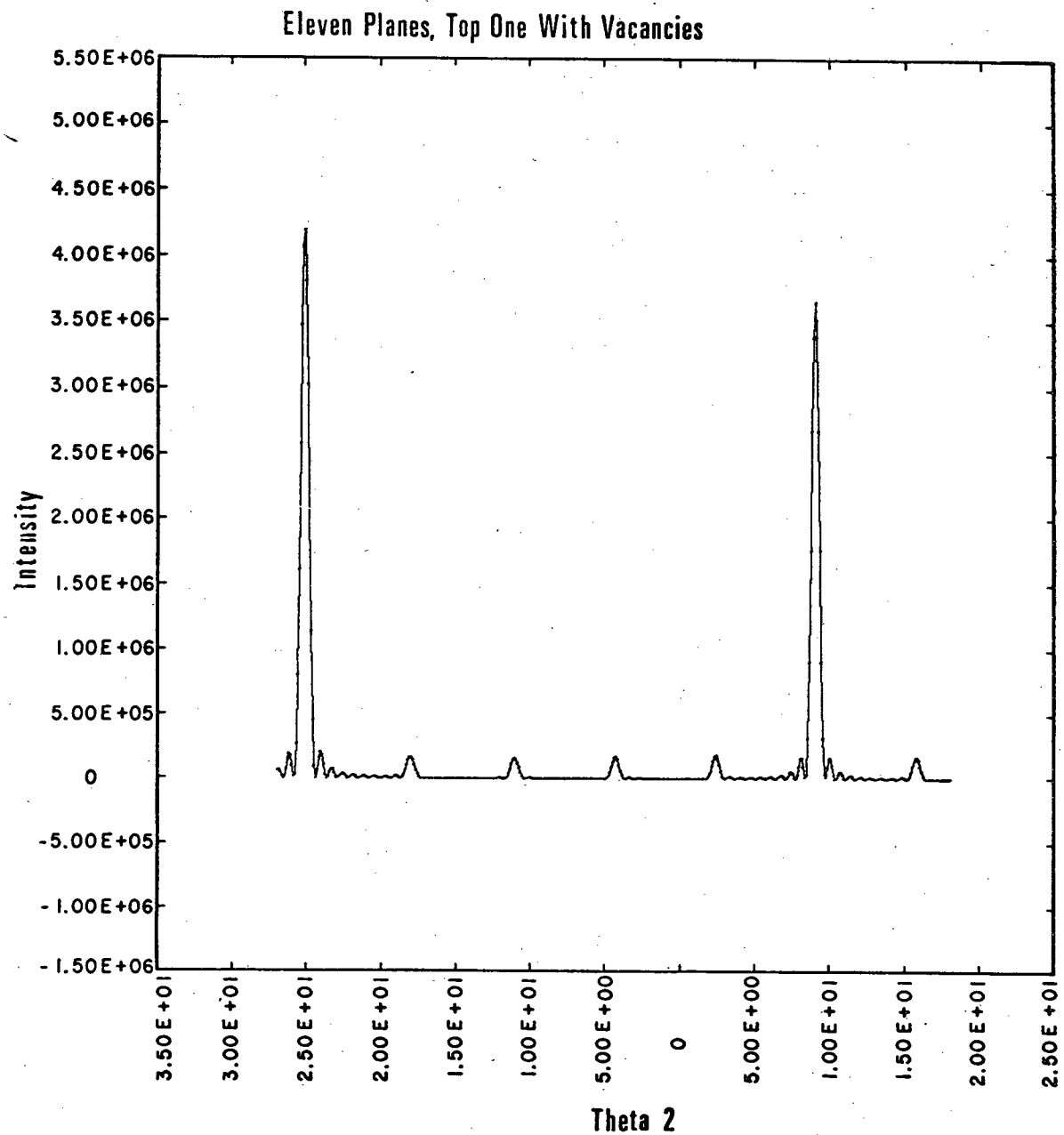

Figure 5.
Computed intensity distribution corresponding to Figure 4 for the case of surface atoms with $z_T = 1.962\text{Å}$ and $f(\theta) = 1$.

XBL 673-1324

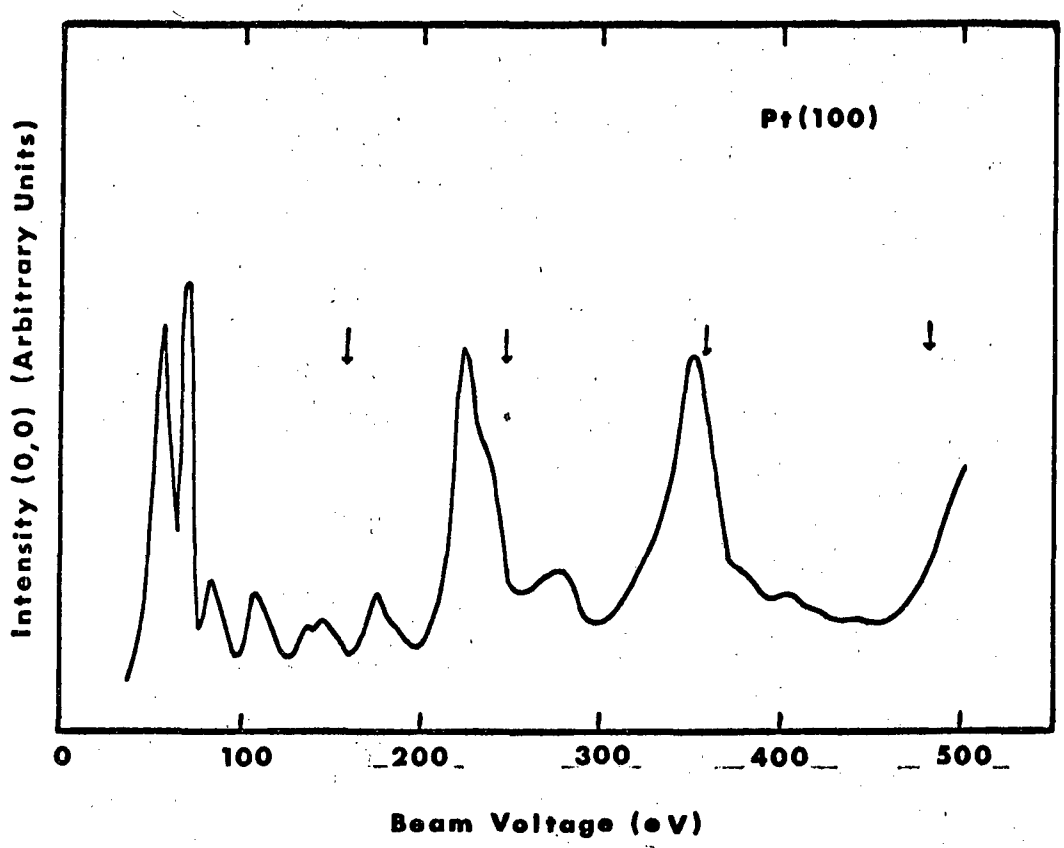

Figure 6. Experimental variation of I_{00} with beam voltage for a clean Pt(100) surface. The incident angle is ~ 12°. Arrows indicate positions of the computed Bragg peaks.

This report was prepared as an account of Government sponsored work. Neither the United States, nor the Commission, nor any person acting on behalf of the Commission:

A. Makes any warranty or representation, expressed or implied, with respect to the accuracy, completeness, or usefulness of the information contained in this report, or that the use of any information, apparatus, method, or process disclosed in this report may not infringe privately owned rights; or

B. Assumes any liabilities with respect to the use of, or for damages resulting from the use of any information, apparatus, method, or process disclosed in this report.

As used in the above, "person acting on behalf of the Commission" includes any employee or contractor of the Commission, or employee of such contractor, to the extent that such employee or contractor of the Commission, or employee of such contractor prepares, disseminates, or provides access to, any information pursuant to his employment or contract with the Commission, or his employment with such contractor.